Mode-based analysis of silicon nanohole arrays for photovoltaic applications

Justin L. Donnelly,[1] Björn C. P. Sturmberg,[1,*] Kokou B. Dossou,[2] Lindsay C. Botten,[2,3] Ara A. Asatryan,[2] Christopher G. Poulton,[2] Ross C. McPhedran,[1] and C. Martijn de Sterke[1]

[1] *CUDOS and IPOS, School of Physics, University of Sydney, 2006, Australia*
[2] *CUDOS, School of Mathematical Sciences, UTS, Sydney, 2007, Australia*
[3] *National Computational Infrastructure, Australian National University, Canberra, Australia*

[*] *b.sturmberg@physics.usyd.edu.au*

Abstract: We investigate the optical properties of silicon nanohole arrays for application in photovoltaic cells in terms of the modes within the structure. We highlight three types of modes: fundamental modes, important at long wavelengths; guided resonance modes, which enhance absorption for wavelengths where the intrinsic absorption of silicon is low; and channeling modes, which suppress front-surface reflection. We use this understanding to explain why the parameters of optimized nanohole arrays occur in specific ranges even as the thickness is varied.

OCIS codes: (350.6050) Solar energy; (310.6628) Subwavelength structures, nanostructures; (050.5298) Photonic crystals.

References and links

1. G. Masson, M. Latour, M. Rekinger, I.-T. Theologitis, and M. Papoutsi, "Global Market Outlook for Photovoltaics 2013-2017," European Photovoltaic Industry Association (2013), http://www.epia.org/news/publications/global-market-outlook-for-photovoltaics-2013-2017/.
2. K. R. Catchpole and A. Polman, "Plasmonic solar cells," Opt. Express **16**, 21793–21800 (2008).
3. H. Ossenbrink, T. Huld, A. Jäger Waldau, and N. Taylor, "PV Electricity Cost Maps," http://iet.jrc.ec.europa.eu/remea/sites/remea/files/reqno_jrc83366_jrc_83366_2013_pv_electricity_cost_maps.pdf.
4. M. K. Dawood, T. H. Liew, P. Lianto, M. H. Hong, S. Tripathy, J. T. L. Thong, and W. K. Choi, "Interference lithographically defined and catalytically etched, large-area silicon nanocones from nanowires," Nanotechnology **21**, 205305 (2010).
5. Q. G. Du, C. H. Kam, H. V. Demir, H. Y. Yu, and X. W. Sun, "Enhanced optical absorption in nanopatterned silicon thin films with a nano-cone-hole structure for photovoltaic applications," Opt. Lett. **36**, 1713–1715 (2011).
6. L. Hu and G. Chen, "Analysis of optical absorption in silicon nanowire arrays for photovoltaic applications," Nano Lett. **7**, 3249–3252 (2007).
7. K. Seo, M. Wober, P. Steinvurzel, E. Schonbrun, Y. Dan, T. Ellenbogen, and K. B. Crozier, "Multicolored vertical silicon nanowires," Nano Lett. **11**, 1851–1856 (2011).
8. B. C. P. Sturmberg, K. B. Dossou, L. C. Botten, A. A. Asatryan, C. G. Poulton, R. C. McPhedran, and C. M. de Sterke, "Nanowire array photovoltaics: Radial disorder versus design for optimal efficiency," Appl. Phys. Lett. **101**, 173902 (2012).
9. C. Lin and M. L. Povinelli, "Optical absorption enhancement in silicon nanowire arrays with a large lattice constant for photovoltaic applications," Opt. Express **17**, 19371–19381 (2011).
10. C. Lin and M. L. Povinelli, "Optical absorption enhancement in silicon nanowire and nanohole arrays for photovoltaic applications," Proc. SPIE **7772**, 77721G (2010).
11. S. E. Han and G. Chen, "Optical absorption enhancement in silicon nanohole arrays for solar photovoltaics," Nano Lett. **10**, 1012–1015 (2010).
12. G. Gomard, R. Peretti, S. Callard, X. Meng, R. Artinyan, T. Deschamps, P. R. i Cabarrocas, E. Drouard, and C. Seassal, "Blue light absorption enhancement based on vertically channelling modes in nano-holes arrays," Appl. Phys. Lett. **104**, 051119 (2014).

#213381 - $15.00 USD Received 3 Jun 2014; revised 14 Jul 2014; accepted 4 Aug 2014; published 14 Aug 2014

13. G. Gomard, E. Drouard, X. Letartre, X. Meng, A. Kaminski, A. Fave, M. Lemiti, E. Garcia-Caurel, and C. Seassal, "Two-dimensional photonic crystal for absorption enhancement in hydrogenated amorphous silicon thin film solar cells," J. Appl. Phys. **108**, 123102 (2010).
14. A. Bozzola, M. Liscidini, and L. C. Andreani, "Photonic light-trapping versus Lambertian limits in thin film silicon solar cells with 1D and 2D periodic patterns," Opt. Express **20**, A224–A244 (2012).
15. F. Wang, H. Yu, J. Li, S. Wong, X. W. Sun, X Wang, and H Zheng, "Design guideline of high efficiency crystalline Si thin film solar cell with nanohole array textured surface," J. Appl. Phys. **109**, 084306 (2011).
16. K.-Q. Peng, X Wang, L Li, X.-L. Wu, and S.-T. Lee, "High-performance silicon nanohole solar cells," J. Am. Chem. Soc. **132**, 6873 (2010).
17. M. Kroll, S. Fahr, C. Helgert, C. Rockstuhl, F. Lederer, and T. Pertsch, "Employing dielectric diffractive structures in solar cells: a numerical study," Phys. Stat. Solidi A **205**, 2777–2795 (2008).
18. M. A. Green and M. J. Keevers, "Optical properties of intrinsic silicon at 300 K," Prog. Photovolt: Res. Appl. **3**, 189 (1995).
19. E. D. Palik, *Handbook of Optical Constants of Solids* (Elsevier, 1991).
20. Available from: http://emustack.com/
21. K. B. Dossou, L. C. Botten, A. A. Asatryan, B. C. P. Sturmberg, M. A. Byrne, C. G. Poulton, R. C. McPhedran, and C. M. de Sterke, "Modal formulation for diffraction by absorbing photonic crystal slabs," J. Opt. Soc. Am. A **29**, 817–831 (2012).
22. American Society for Testing Materials, "Reference Solar Spectral Irradiance: Air Mass 1.5 Spectra," http://rredc.nrel.gov/solar/spectra/am1.5/.
23. W. Shockley and H. J. Queisser, "Detailed balance limit of efficiency of pn junction solar cells," J. Appl. Phys. **29**, 510–519 (1961).
24. The parameter $\kappa_j = |(\mathbf{T}_{12})_{j,0}|^2$ where $\mathbf{T}_{12}$ is the transmission scattering matrix that couples light from air to the nanohole array (see Ref. [25]). Index 0 labels incident plane wave.
25. B. C. P. Sturmberg, K. B. Dossou, L. C. Botten, A. A. Asatryan, C. G. Poulton, C. M. de Sterke, and R. C. McPhedran, "Modal analysis of enhanced absorption in silicon nanowire arrays," Opt. Express **19**, 1064–1081 (2011).
26. L. Genzel and T. P. Martin, "Infrared absorption by surface phonons and surface plasmons in small crystals," Surf. Sci. **34**, 33–49 (1973).
27. N. M. Litchinitser, S. C. Dunn, P. E. Steinvurzel, B. J. Eggleton, T. P. White, R. C. McPhedran, and C. M. de Sterke, "Application of an ARROW model for designing tunable photonic devices," Opt. Express **12**, 1540–1550 (2004).

1. Introduction

Generating electricity from sunlight via photovoltaic (PV) cells is an increasingly important alternative to the combustion of fossil fuels. Despite recent growth, PV cells produce only a small fraction of global energy supply; in 2012, 2.6% of the European Union's power was generated by PV cells [1]. The key barrier to greater adoption of photovoltaics is cost. For current silicon (Si) PV cells, which constitute more than 80% of the market, 40% of the PV module cost is due to the use of high purity Si [2]. While the cost of PV modules has been brought down to account for 19% of the total costs of installed PV systems [3], further cost reductions will increase the rate of investment and installation. Conventional SiPV cells typically have thicknesses of 200 μm to ensure adequate broadband absorption, which requires the Si to be of high purity for efficient charge-carrier extraction.

An approach to significantly reducing the cost of Si PVs is to use thin absorbing layers. However silicon is an indirect band-gap semiconductor and absorbs poorly across a substantial range of the solar spectrum, particularly at wavelengths near its electronic band-gap at $\lambda_g = 1127$ nm. To create an efficient thin film SiPV device it is therefore necessary to introduce light trapping elements to increase the absorption. Potential nanostructures that have been shown to strongly enhance absorption include nanocones [4], nano-cone-holes [5], nanowire (NW) arrays [6–9], and nanohole arrays [10–16]. Nanowire arrays in particular have been the focus of much theoretical and experimental work. The absorption enhancement in NW arrays has been shown to occur due to strong coupling to resonant modes that are concentrated within the silicon NWs [7].

Here we investigate arrays of air *nanoholes* (NH) in an otherwise uniform layer of silicon

#213381 - $15.00 USD Received 3 Jun 2014; revised 14 Jul 2014; accepted 4 Aug 2014; published 14 Aug 2014

(see Fig. 1(a)), *i.e.* structures which are complementary to nanowire arrays. Earlier numerical studies of NH arrays have shown that arrays of thickness 2.33 μm can out-perform optimal nanowire arrays in terms of ultimate efficiency [10,11], and that arrays perform well over a large range of incident angles [10]. NH array absorption enhancement has been shown to occur via antireflection, in particular due to channeling modes concentrated in low index NHs [12], and guided resonance modes, a bulk property of NH arrays that produce sharp peaks in absorption spectra [10,13,14]. Numerical studies have also shown the electrical performance of NH arrays to be superior to NW arrays [15]. NH array PV cells with efficiencies exceeding 10% have been experimentally demonstrated [16].

We study the modes of the NH arrays in detail which is enabled by having direct access to the Bloch modes of the NH arrays. Our mode based analysis complements previous studies of nano-structured PVs: Kroll et al. identified key mechanisms for absorption enhancement [17], but did not have access to the same modal information. We show how NH array modes differ significantly from those of NW arrays; for NW arrays the properties of the guided modes in the high index rods essentially determine the propagation and absorption of light in the system, whereas this is not so for nanoholes in which the inclusion has the low refractive index.

After a brief discussion of our approach in Section 2, we elucidate the characteristics of the three types of modes in Section 3. We use this understanding in Section 4 to explain an optimization of the ultimate efficiency of NH arrays with thicknesses 0.5 μm, 2.33 μm, and 5.0 μm. In Section 5 we discuss our results and conclude.

2. Approach

We calculate the absorption of a silicon [18] layer patterned with a square lattice of circular air holes. The depth of these holes is equal to the thickness of the silicon layer, as shown in Fig. 1(a). The NH arrays are characterized by a lattice period d and hole radius r, so that the air volume fraction is $f = \pi r^2/d^2$. The NH arrays are modeled with an air superstrate and silica glass [19] substrate. We present a structure with a simple silica glass substrate, so that discussion is focused solely on understanding the optical properties of the silicon layer. Cells fabricated using Si NH arrays have a more complex structure than that presented here, as charge carrier extraction is required and a back reflector may be included.

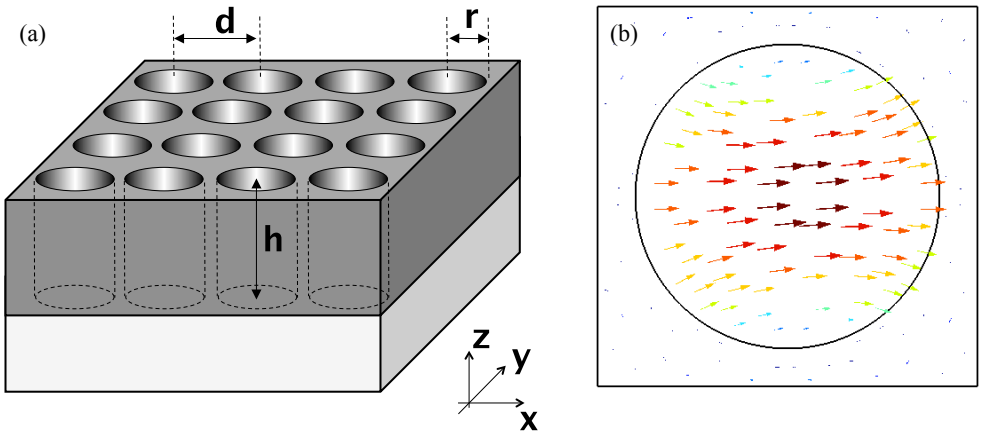

Fig. 1. (a) Square NH array structure; with air NHs, silicon matrix and silica glass substrate. NH arrays are parameterized by period d, radius r and height h. (b) Electric field distribution for the channelling Bloch mode discussed in Sect. 3.3.

#213381 - $15.00 USD Received 3 Jun 2014; revised 14 Jul 2014; accepted 4 Aug 2014; published 14 Aug 2014

Simulations were performed using the freely available EMUstack package [20], which implements a semi-analytic scattering matrix method [21]. EMUstack calculates the Bloch modes of the NH array using a 2D vectorial Finite Element Method (FEM) routine. This provides direct access to the propagation constants, field distributions and cut-offs of the Bloch modes. As an example Fig. 1(b) shows the electric field distribution of the channelling Bloch mode (see Sect. 3.3). These Bloch modes propagate in the $\pm z$ directions. EMUstack next calculates the coupling of the incident plane waves directly into the individual Bloch modes of the array, from which the absorption of a semi-infinite array can be evaluated. We use between $50-400$ Bloch modes to achieve the numerical convergence described in [21]. The properties of arrays of finite thickness are found by coupling the Bloch modes back into plane waves at the bottom of the structured layer. The modal formulation of our method allows for better physical insight than purely numerical approaches such as Finite Difference Time Domain, as we can isolate the effect of individual Bloch modes, a feature which is used extensively in Section 3.

We use the *ultimate efficiency* η to evaluate the photovoltaic performance of NH arrays:

$$\eta = \frac{\int_{\lambda_l}^{\lambda_g} I(\lambda) A(\lambda) \frac{\lambda}{\lambda_g} d\lambda}{\int_{\lambda_l}^{\lambda_u} I(\lambda) d\lambda}, \tag{1}$$

where $\lambda_l = 310$ nm is the lower edge of the solar emission spectrum and $\lambda_u = 4000$ nm is its upper edge. $I(\lambda)$ is the incident solar irradiance given by the 1.5 air mass solar spectrum [22], $A(\lambda)$ is the optical absorptance of the NH array and λ_g is the free space wavelength of light with bandgap energy E_g. The ultimate efficiency is the idealized energy conversion efficiency of a solar cell in which each absorbed photon is taken to produce a hole-electron pair with an external voltage corresponding to E_g [23]. The only loss mechanism included in η is therefore the thermalization of charge-carriers to the electronic band edge.

3. Modal analysis of light propagation in nanohole arrays

While NH arrays support many Bloch modes, for most frequencies in the solar spectrum only a small number of these significantly contribute to energy transport and absorption. The importance of a Bloch mode j can be quantified by the coupling coefficient κ_j [24] into that mode from an incident plane wave, which we here take to be normally incident. In this way it is found that the optical properties of NH arrays are largely determined by three types of modes, the degenerate *fundamental Bloch modes*, *guided resonance modes* (which are superpositions of upwards and downwards propagating Bloch modes) and the *channeling Bloch modes*, which are discussed in Subsections 3.1, 3.2 and 3.3, respectively.

Since absorption only occurs in silicon, one metric to characterize the absorptance of a Bloch mode is the fraction of that mode's electric field concentrated in silicon,

$$\zeta = \frac{\int_{\text{silicon}} \|\mathbf{E}\|^2 dA}{\int_{\text{unit cell}} \|\mathbf{E}\|^2 dA}, \tag{2}$$

where $\|\mathbf{E}\|$ is the electric field magnitude. We find that the field concentration is an appropriate measure to explain the absorption of fundamental modes and the channeling modes.

In Fig. 2, we show for which propagation constants and frequencies these modes exist, where $\|\beta_{1,0}\| = 2\pi/d$ is the wavevector magnitude in the plane of periodicity. Equivalently, the top axis in Fig. 2 shows the periods at which modes can be excited for normally incident light. This figure will be discussed in detail in the following subsections.

#213381 - $15.00 USD Received 3 Jun 2014; revised 14 Jul 2014; accepted 4 Aug 2014; published 14 Aug 2014

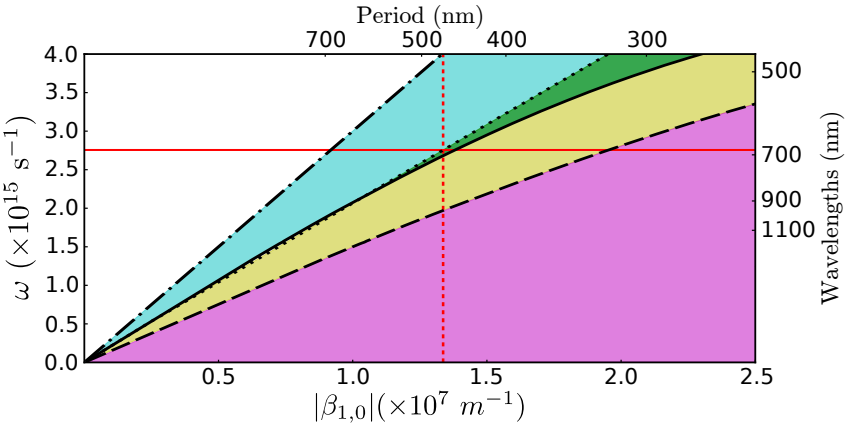

Fig. 2. Frequency and wavenumber dependence of fundamental, guided resonance and channeling modes in NH arrays with 60% volume fraction. Top axis: period corresponding to the first order reciprocal lattice vector needed to excite the mode. The black dot-dashed, dotted and dashed lines give the cut-offs of first diffraction order in air, silica glass and a silicon NH array of $f = 60\%$. The black solid curve approximates the cut-off of the channeling modes (Eq. (5)). Magenta region: only fundamental modes supported; yellow region: guided resonance modes supported; cyan region: channeling modes supported; green region: both guided resonance and channeling modes supported. Horizontal red solid line: $\lambda = 684$ nm, for which $\alpha h = 0.5$ for a silicon slab of thickness $h = 2.33$ μm. Vertical red dashed line: period $d = 470$ nm, where horizontal line intersects the dotted black curve.

3.1. Fundamental modes

NH arrays support a degenerate pair of fundamental Bloch modes at all wavelengths, which have a zero wavevector component in the plane of the array. This pair of modes have electric field distributions connected by an angular rotation of 90° in this plane, with the degeneracy arising from the symmetry of the array. At sufficiently long wavelengths fundamental modes are the only relevant propagating Bloch modes, because all other Bloch modes have negligible coupling to the incident plane waves. The cut-off of the next relevant set of modes can be estimated as follows: drawing from grating theory, we associate the specular diffraction order in the NH array with the array's fundamental Bloch modes. Similarly, we associate the next set of modes with the first diffracted order in the array. According to standard grating theory, at normal incidence the first diffracted order is supported only for wavelengths $\lambda < \lambda_1$, where

$$\lambda_1 = \mathrm{Re}(n_{\mathrm{eff}})d, \tag{3}$$

where n_{eff} is an appropriate effective refractive index of the medium. We have found that the cut-off of this diffracted order is remarkably close (within a few percent) to the modal cut-off if n_{eff} is calculated using Maxwell-Garnett theory, according to which, for cylindrical inclusions,

$$n_{\mathrm{eff}} = \sqrt{\varepsilon_b \frac{\varepsilon_i(1+f)+\varepsilon_b(1-f)}{\varepsilon_i(1-f)+\varepsilon_b(1+f)}}, \tag{4}$$

where f is the inclusion (air) volume fraction, and ε_i, ε_b are the dielectric constants of the inclusion and background dielectric, respectively [26]. This agreement is surprising since Maxwell-Garnett theory typically applies to structures with small f and for $d \ll \lambda$. The black dashed

#213381 - $15.00 USD Received 3 Jun 2014; revised 14 Jul 2014; accepted 4 Aug 2014; published 14 Aug 2014

curve in Fig. 2 indicates λ_1, for $f = 60\%$. The magenta shaded region in Fig. 2 indicates wavelengths $\lambda > \lambda_1$, where the fundamental Bloch modes are the only relevant modes. We conclude that the fundamental modes are particularly important for small-period arrays.

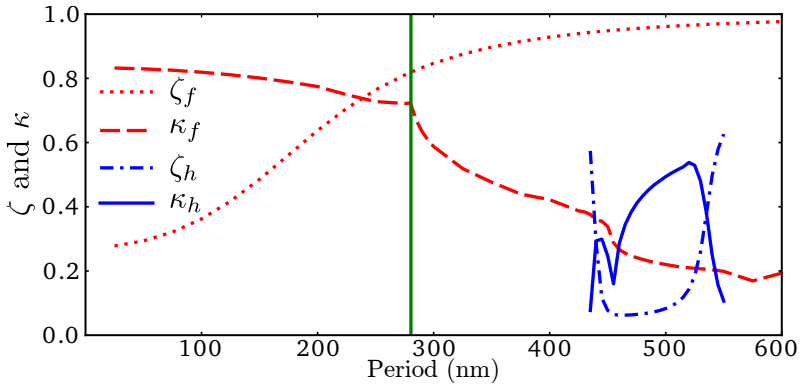

Fig. 3. Coupling constants of the fundamental (κ_f, red dashed curve) and channeling modes (κ_h, blue solid curve) together with the field concentrations of the fundamental (ζ_f, red dotted curve) and channeling modes (ζ_h, blue dot-dashed curve) for $\lambda = 669$ nm in NH arrays with $f = 50\%$, versus period d. The green vertical line is the cut-off Eq. (3).

Figure 3 gives the variation of the key parameters of the fundamental mode with NH period d for incident light of $\lambda = 669$ nm, corresponding to the peak of the solar photon flux. The coupling coefficient κ (red dashed curve) in Fig. 3 shows the total energy in both degenerate fundamental modes. Note the strong coupling for periods $d < 669$ nm$/n_{\text{eff}} = 280$ nm, where the fundamental modes are the only relevant modes; this coupling reduces considerably beyond the cut-off of the first diffracted order Eq. (3). The red dotted curve in Fig. 3 gives the field concentration ζ and shows that as the period increases, the fundamental mode field increasingly localizes in the silicon, being almost entirely concentrated there for $d > 400$ nm.

Figure 4 shows the absorptance versus wavelength for NH arrays with $f = 50\%$ and $h = 2.33$ μm for $d = 25$ nm (blue curve), $d = 200$ nm (red dotted curve), and $d = 500$ nm (black dashed curve). For the array with period $d = 25$ nm the fundamental modes are the only relevant modes for the entire spectrum shown, while for period $d = 200$ nm this is so only for wavelengths $\lambda > 518$ nm. For $d = 500$ nm additional modes propagate over the entire spectrum shown. The first two curves exhibit smooth Fabry-Perot fringes, consistent with the notion that a single pair of degenerate Bloch modes dominates the light propagation. In this spectral region the absorption in the $d = 200$ nm array is always larger than that in the array with $d = 25$ nm; this is consistent with our earlier finding that the field is more concentrated in the silicon at larger periods. For short wavelengths the fringes disappear because the layer is optically thick. Thus NH arrays with very short periods are not useful for photovoltaic applications as the light is not sufficiently concentrated in the silicon to deliver strong absorption.

The array of period $d = 500$ nm is multi-moded for all wavelengths in Fig. 4. While its absorption is larger than that of the arrays with the smaller periods, its spectrum differs in two key ways. The first is that the smooth Fabry-Perot features are superimposed to sharp resonances for $\lambda > 700$ nm. These are due to guided resonance modes, discussed in Subsection 3.2. The second difference is the low absorption at $\lambda \approx 700$ nm. This is associated with the channeling mode to be discussed in Subsection 3.3.

#213381 - $15.00 USD Received 3 Jun 2014; revised 14 Jul 2014; accepted 4 Aug 2014; published 14 Aug 2014

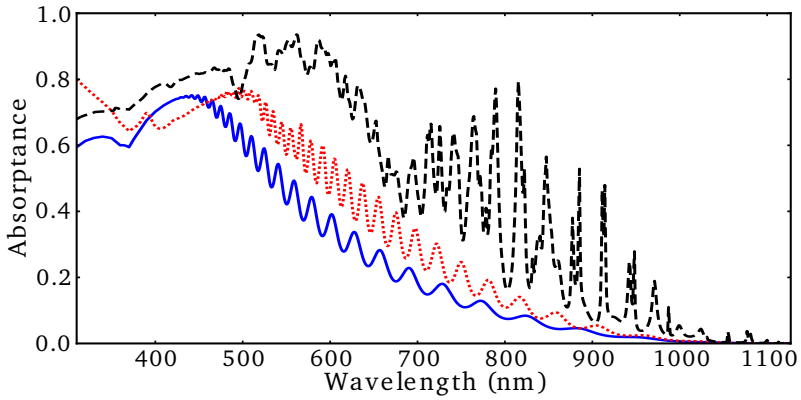

Fig. 4. Absorption spectra of NH arrays with $f = 50\%$ and $h = 2.33$ μm. The blue solid line is the absorptance of an array with $d = 25$ nm, the red dotted line $d = 200$ nm and the black dashed line $d = 500$ nm

3.2. *Guided resonance modes*

A NH array resembles a planar dielectric waveguide, with a high index air-silicon composite medium between an air superstrate and silica substrate. The high index composite layer can support guided resonance modes bound by total internal reflection, provided the losses are not too high [10, 13, 17]. These modes can be excited from the air by exploiting the hole array, which acts like a conventional grating coupler. Exciting such modes enhances absorption as they propagate parallel to the layer.

Guided resonance modes only exist if the absorption is sufficiently low for constructive interference to occur over the thickness of the waveguide. This motivates our criterion that guided resonance modes can enhance absorption when $\alpha h < 0.5$, with α the attenuation constant of bulk silicon. For NH arrays of thickness $h = 2.33$ μm, this condition is met for $\lambda > 684$ nm; absorption enhancement by guided resonance modes becomes increasingly important for thinner arrays. Of course when the losses are so high that guided resonance modes do not form then the transmission is negligible and reflection management is required to optimize absorption.

Guided resonance modes are indicated in Fig. 2 showing frequency versus wavenumber (top and right axes). The horizontal red solid line in Fig. 2 is at $\lambda = 684$ nm, for shorter wavelengths above this line absorption is so high that guided resonance modes do not form for $h = 2.33$ μm. The light lines of silica glass, and air are given by the black dotted and dot-dashed curves respectively. The light line of a NH array with $f = 60\%$ is approximated by the black dashed line (Eq. (3) and (4)). A guided resonance mode is bound when its frequency and wavenumber are between the array light line and the silica light line, the yellow and green regions of Fig. 2, since above the silica light line no total internal reflection occurs and below the array light line the field is evanescent.

We consider a NH array with an incident plane wave normal to the interfaces, for which the in-plane component of the wavevector vanishes. The periodic NH array can couple the light into a guided resonance mode with in-plane wavevector $\beta_{p_x p_y} = \mathbf{G}_{p_x p_y} = \frac{2\pi}{d}(p_x \hat{\mathbf{x}} + p_y \hat{\mathbf{y}})$, where $p_{x,y}$ are integers. For a given period, $\mathbf{G}_{\pm 10}$ and $\mathbf{G}_{0\pm 1}$ are the shortest and most effective reciprocal lattice vectors. The vertical red dashed line in Fig. 2 is the $\mathbf{G}_{\pm 10}$ of an array with period $d = 470$ nm. The in-plane component of the wavevector β of this line is significant because it intersects the silica light line at $\lambda = 684$ nm and hence this array supports guided resonance modes in the spectral region where they provide the greatest benefit.

Guided resonance modes provide absorption enhancement at frequencies where the intrinsic

#213381 - $15.00 USD Received 3 Jun 2014; revised 14 Jul 2014; accepted 4 Aug 2014; published 14 Aug 2014

absorption of silicon is low, and most light would otherwise be transmitted through the NH array. They lead to the sharp resonances in the black dashed curve in Fig. 4. Figure 5 shows the reflectance, absorptance and transmittance of NH arrays of period $d = 500$ nm and air volume fraction $f = 50\%$. Three of the arrays studied have finite thickness $h = 0.5$ μm (green dotted curve), $h = 2.33$ μm (blue solid curve) and $h = 5$ μm (red dash-dotted curve), and the other is semi-infinite, *i.e.*, $h \to \infty$ (black dashed curve); this means that all light that is not reflected by the top surface is absorbed.

3.3. Channeling modes

Nanohole arrays with periods $d \approx \lambda$ can support Bloch modes that are strongly concentrated in the air holes as shown in Fig. 1(b) [12]. Like the fundamental modes these channeling modes come in degenerate pairs. Since the field in these modes is predominantly concentrated in air we expect that the absorption of light is low. Moreover, because the field is concentrated in air, the impedance of these modes is similar to that of air, so the coupling into these modes can be expected to be substantial [14, 17]. Both of these properties are illustrated in Fig. 3, which shows how the channeling modes' field concentration in silicon (ζ_h, blue dot-dashed curve) and the coupling (κ_h, blue solid curve) depend on period. The channeling modes are evanescent at $\lambda = 669$ nm for arrays with $f = 50\%$ and $d < 454$ nm. Figure 3 shows that the coupling strength of the channeling modes obtains a local minimum at the point, $d = 454$ nm, where transition from propagating to evanescent occurs. Figure 3 also shows an increase in the coupling strength of the fundamental modes at periods $d < 454$ nm where the channeling mode is evanescent.

Figure 5 confirms that all but the very thinnest structures exhibit low reflection for light of wavelengths $500\text{ nm} < \lambda < 731$ nm. The short wavelength edge of this trough is again explained by grating theory: the first reflected diffraction order (in air) cuts-off at $\lambda = d$; thus for longer wavelengths only the specular reflection order is supported, leading to low reflection. The long wavelength edge of the trough coincides with the cut-off of the channeling mode, which may be roughly approximated by

$$\lambda_h = \mathrm{Re}(n_{\mathrm{eff}})d/\sqrt{2}, \tag{5}$$

where n_{eff} is the Maxwell Garnett effective refractive index of the medium. The difference between the Bloch mode cut-off accurately calculated in EMUstack and the approximation Eq. (5) is less than 15%. The presence of the $\sqrt{2}$ factor in Eq. (5) suggests that the channeling modes are associated with the NH array's second diffraction order, coupled by the $\mathbf{G}_{\pm1\pm1}$ reciprocal lattice vector. For wavelengths $\lambda > \lambda_h$ the channeling mode is not supported, leading to increased reflection. In Fig. 2, $\lambda = \lambda_h$ is given by the black solid curve, while $\lambda = d$ is given by the black dot-dashed line. The cyan and green shaded areas between these two curves, $d < \lambda < \lambda_h$, give the spectral region over which channeling modes are important.

Light propagating in channeling modes is absorbed weakly because of these modes' high field concentration in air (see Fig. 1(b) and Fig. 3). Depending on the thickness, channeling modes thus can have either a positive (anti-reflection) or negative (transmission) effect on the absorption of NH arrays. Figure 5 illustrates this trade-off. For thin arrays (thickness $h = 0.5$ μm and $h = 2.33$ μm), the lower absorption of the channeling modes is detrimental, with energy lost to transmission. For the semi-infinite structure all light that enters the array is absorbed and the channeling modes provide anti-reflection benefits. Though for the array of intermediate thickness ($h = 5$ μm) the light coupled to the channeling mode is not entirely absorbed, the low reflection has a small net positive impact on the absorption (see Fig. 5(b)). While the presence of channeling modes is beneficial for thick arrays, increasing the thickness may not be desirable. Alternative ways to reduce losses via channeling mode transmission are to have hole depths less than the thickness of the silicon layer (investigated by Gomard et al. [12]) or to shift the channeling mode cut-off to shorter wavelengths where the intrinsic absorption of

#213381 - $15.00 USD Received 3 Jun 2014; revised 14 Jul 2014; accepted 4 Aug 2014; published 14 Aug 2014

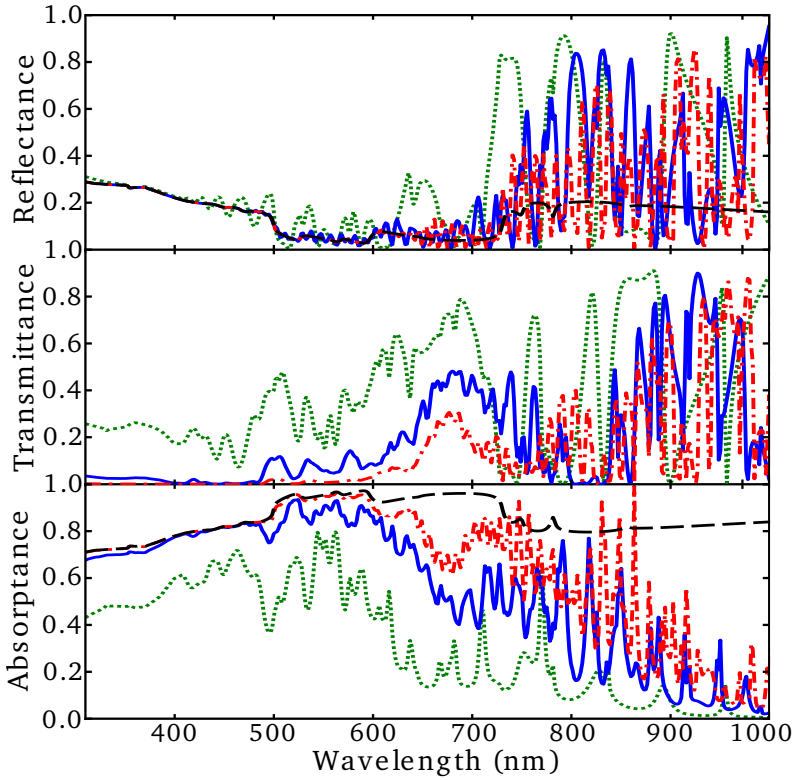

Fig. 5. Reflection, transmission and absorption spectra for silicon NH arrays with period $d = 500$ nm and air volume fraction $f = 50\%$, with an air superstrate and silica substrate. The green dotted curve for thickness $h = 0.5$ μm, the blue solid curve for $h = 2.33$ μm, the red dot-dashed curve is for $h = 5$ μm, and the black dashed line is for a semi-infinite array. The spectra are shown for $\lambda < 1000$ nm with the spectra becoming too complicated at larger wavelengths to be of use. This region of the spectra has low integrated absorptance, and is a negligible component of ultimate efficiency.

silicon is higher. To take advantage the latter option, an understanding of how the channeling mode cut-off wavelength varies with array parameters is required.

Estimate (5) shows that the cut-off wavelength of the channeling modes depends on NH array period d, and, via n_{eff}, on the air volume fraction f. Figure 2 shows that we can shift the channeling mode cut-off to shorter wavelengths by using arrays with smaller periods. We found that the NH radius in itself does not affect λ_h: for constant period, λ_h decreases with increasing radius, whereas for constant air volume fraction, λ_h increases with radius. Thus the channeling modes of NH arrays are unlike the key modes in nanowire arrays, which are also strongly concentrated in the inclusions, but whose cut-offs scale with nanowire radius, not with the period and volume fraction [8].

Understanding the three relevant mode types in a NH array allows us to increase its absorption. The properties of the fundamental mode show the need to avoid small periods. The period needs to be sufficiently long to ensure coupling to a large number of guided resonance modes. Finally, the cut-off of the channeling modes needs to be in the wavelength range where silicon strongly absorbs, so that their antireflection properties can be exploited. These ideas are further developed in Section 4.

#213381 - $15.00 USD Received 3 Jun 2014; revised 14 Jul 2014; accepted 4 Aug 2014; published 14 Aug 2014

We studied NH arrays $0.5-5$ μm thick as this thickness range provides the best chance to demonstrate the described trade-offs associated with channeling modes. At greater thicknesses large air volume fraction f is always desirable, while for smaller thicknesses transmission is too great.

4. Ultimate efficiency

Having discussed the three main types of modes in NH arrays, we now show how these affect the ultimate efficiency η (Eq. (1)). Figure 6 shows the ultimate efficiency versus period and air volume fraction for silicon arrays with a silica glass substrate and an air superstrate and a thickness of (a) $h = 0.5$ μm; (b) $h = 2.33$ μm; and (c) $h = 5.0$ μm. The optimal efficiencies are 14.0%, 24.0% and 28.8% when $h = 0.5$ μm, 2.33 μm, 5 μm respectively. This highlights the advantage of NH arrays to trap light in thin films. In all figures the curves of equal ultimate efficiency run approximately vertically for small periods, and run approximately horizontally for small air volume fractions. This can be understood as follows: at small periods ($d < 250$ nm) the only relevant modes are the fundamental modes, for which the electric field is almost entirely concentrated in the silicon, leaving a weak dependence on the air volume fraction. Similarly, at low air volume fractions ($f < 20\%$) the structure homogenizes according to Eq. (4), and the value of the period is of secondary importance. For all three thicknesses the ultimate efficiency peaks for periods in the range of $d = 400-600$ nm and air volume fraction $f = 40-60\%$. The positions and values for the various local and global maxima are indicated by green dots in Fig. 6 and are summarized in Table 1.

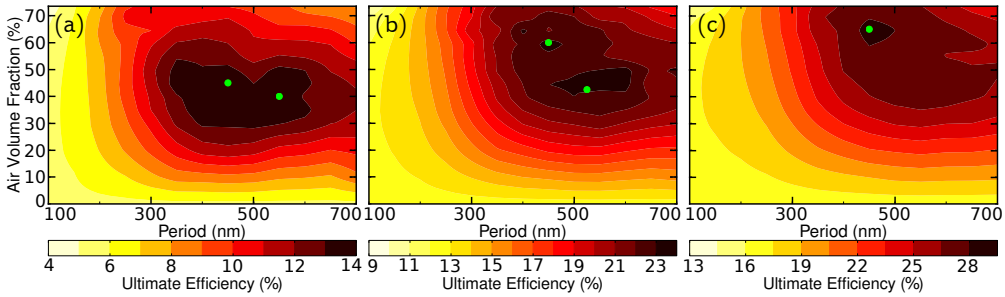

Fig. 6. Ultimate efficiency of NH arrays with a thickness of (a) $h = 0.5$ μm; (b) $h = 2.33$ μm; (c) $h = 5.0$ μm versus period and air volume fraction. Green dots indicate local maxima.

Table 1. For three thicknesses h, the values for period d and air volume fraction f giving the local and global (bold) maxima in ultimate efficiency η.

h (μm)	d (μm)	f (%)	η (%)
0.5	450	45	**14.0**
0.5	550	40	13.9
2.33	525	42.5	**24.0**
2.33	450	60	23.4
5.0	450	65	**28.8**

An obvious trend from the table is that the optimal air volume fraction increases with thickness. This is so because for thin structures it is paramount to have sufficient silicon to absorb the

#213381 - $15.00 USD Received 3 Jun 2014; revised 14 Jul 2014; accepted 4 Aug 2014; published 14 Aug 2014

light, even if this increases reflection losses. Similarly, for thick structures with more absorbing material it is more important to reduce reflection losses by increasing the air volume fraction. Understanding the optimal periods is more subtle. The clustering of their values around 450 nm and 550 nm provides a clue, however.

A period of $d = 550$ nm ensures that the center of the low-reflectivity region due to the presence of the channeling mode coincides with the maximum of the solar photon flux. In this way the reflectivity over the most intense part of the solar emission spectrum is minimized (perhaps at the expense of increased transmission).

A period of $d = 450$ nm is close to the vertical red dashed line in Fig. 2. Consider the horizontal dash-dotted line which marks the region where absorption dominates at shorter wavelengths, from the region where propagation effects dominate at longer wavelengths. At the shorter wavelengths, it is imperative that reflection be minimized by channeling modes, whereas at the longer wavelengths the presence of guided resonance modes is required to enhance the absorption. A period around $d = 450$ nm ensures that both these requirements are simultaneously satisfied. For all thicknesses, the global features of the ultimate efficiency can be understood from a competition of these two basic effects so the optimum periods come to depend weakly on array thickness. However, the $\alpha h = 0.5$ criterion for the horizontal solid line means that the line shifts to larger wavelengths as the NH array becomes thicker, and the corresponding period vertical line to larger values.

We note that the optimal NH array periods are similar to the optimal periods for NW arrays, but that the optimal air volume fraction is consistently higher by over 10%. We attribute the former of these to both arrays exciting the same diffraction orders in reflection and transmission, with their excitation determined by the grating equation that depends solely on their period. Despite the optimal NH arrays containing less silicon than optimal NW arrays, the NH arrays have an ultimate efficiency approximately 2% higher.

5. Discussion and conclusions

An analysis of the absorption properties of NH arrays is aided by an understanding of the relevant modes in the film layer. Though the fundamental modes dominate the properties of arrays with short periods, the arrays with highest broadband absorption support another two types of modes. The parameters of the optimal arrays balance the effects of guided resonance modes, which increase absorption, and channeling modes which are excited at shorter wavelengths and, though in themselves not leading to strong absorption, reduce reflection. The way channeling modes affect absorption thus depends on the thickness of the film. Even though one might therefore expect that the parameters which lead to optimal absorption vary widely with layer thickness, we found that, for the thicknesses we investigated, the array period takes a value in one of two ranges. In the first the peak of the solar photon emission spectrum falls well inside the region where channeling modes are excited. In the second, the period is such that guided resonance modes are excited in the region of modest intrinsic absorption, whereas channeling modes are excited for wavelengths where the absorption is high.

It is remarkable to note the degree to which these arguments differ from those for NW arrays. In the latter structures the absorption is largely determined by a set of Key Modes, the properties of which, to lowest order, only depend on the diameter of the nanowires [25]. None of the relevant NH modes have this property – as we saw, their properties are mostly determined by the period of the array, whereas the air volume fraction to a large degree determines the reflection off the front surface. This difference of modal properties, with the concomitant difference in absorption properties, arises because a high index inclusion in a low index background has its own modes, whereas low-index inclusion in a high-index background does not. This distinction is similar to that in microstructured optical fibres. There, the properties of fibres with low-index

#213381 - $15.00 USD Received 3 Jun 2014; revised 14 Jul 2014; accepted 4 Aug 2014; published 14 Aug 2014

inclusions in a high-index background differ strongly from those with high-index inclusions in a low-index background [27].

One of the key considerations was the spectral position of the channeling modes with the low reflectivity. It is likely that in designs for inclusion in tandem geometries, where the NH array would be the front cell, spectral positioning of the channeling modes may extend the cell's transmission window.

Acknowledgments

This work was funded by the Australian Renewable Energy Agency and the Australian Research Council through Grant DP130101009.

#213381 - $15.00 USD Received 3 Jun 2014; revised 14 Jul 2014; accepted 4 Aug 2014; published 14 Aug 2014